Atmos. Chem. Phys. Discuss., 15, 27853–27875, 2015
www.atmos-chem-phys-discuss.net/15/27853/2015/
doi:10.5194/acpd-15-27853-2015

Atmospheric Chemistry and Physics Discussions

Development of a new methane tracer: kinetic isotope effect of $^{13}CH_3D$ + OH from 278 to 313 K

L. M. T. Joelsson[1,3], J. A. Schmidt[1], E. J. K. Nilsson[2], T. Blunier[3], D. W. T. Griffith[4], S. Ono[5], and M. S. Johnson[1]

[1]Department of Chemistry, University of Copenhagen, Copenhagen, Denmark
[2]Department of Physics, Combustion Physics, Lund University, Lund, Sweden
[3]Centre for Ice and Climate (CIC), Niels Bohr Institute, University of Copenhagen, Copenhagen, Denmark
[4]Department of Chemistry, University of Wollongong, Wollongong, Australia
[5]Department of Earth, Atmospheric and Planetary Sciences, Massachusetts Institute of Technology, Cambridge, MA, USA

Received: 16 September 2015 – Accepted: 16 September 2015 – Published: 15 October 2015

Correspondence to: M. S. Johnson (msj@kiku.dk)

Published by Copernicus Publications on behalf of the European Geosciences Union.

Abstract

Methane is the second most important long lived greenhouse gas and impacts the oxidative capacity of the Earth's atmosphere. Nontheless there are significant uncertainties in its source budget. Analysis of the isotopic composition of atmospheric methane, including doubly substituted species (e.g. $^{13}CH_3D$), offers new constraints on the methane source budget as the sources and sinks have distinct isotopic signatures. The most important sink of atmospheric methane is oxidation by OH which accounts for around 90 % of methane removal in the troposphere. Here we present experimentally derived methane + OH kinetic isotope effects and their temperature dependence over the range of 278 to 313 K for CH_3D and $^{13}CH_3D$; the latter is reported here for the first time. We find $k_{CH_4}/k_{CH_3D} = 1.31 \pm 0.01$ and $k_{CH_4}/k_{^{13}CH_3D} = 1.34 \pm 0.03$ at room temperature, implying that the methane + OH kinetic isotope effect is multiplicative such that $(k_{CH_4}/k_{^{13}CH_4})(k_{CH_4}/k_{CH_3D}) = k_{CH_4}/k_{^{13}CH_3D}$ to within the experimental uncertainty. In addition the kinetic isotope effect were characterized using transition state theory with tunneling correction. Good agreement between the experimental, quantum chemical and available literature values was obtained. The theoretical calculations show that $^{13}CH_3D$ isotope effects is the product of D- and ^{13}C-isotope effect. Based on the results we conclude that the OH reaction at steady-state can produce an atmospheric clumped isotope signal ($\Delta(^{13}CH_3D) = \ln([CH_4][^{13}CH_3D]/[^{13}CH_4][CH_3D])$) of 0.02 ± 0.02.

1 Introduction

Atmospheric methane is the subject of increasing interest from both the climate research community and the public due its impacts in climate change, as reported by the IPCC (2013). The direct radiative forcing of methane from is $0.64\,W\,m^{-2}$. Including feedback mechanisms and secondary effects e.g. increased O_3 production, stratospheric water vapor and production of CO_2, the radiative forcing becomes

ACPD
15, 27853–27875, 2015

0.97 W m^{-2} (i.e. 2/3 of the forcing by CO_2 over the same time period; IPCC, 2013, Fig. 8.15).

Atmospheric methane has both natural and anthropogenic sources and the two categories contribute about equally (Ciais et al., 2013, and references therein). Wetlands are the dominant natural source, and agriculture and waste are the largest anthropogenic sources. Fossil fuels make smaller contributions. A majority (84 %) of atmospheric methane is removed in the troposphere by oxidation by OH:

$$CH_4 + OH \rightarrow CH_3 + H_2O, \quad \text{(R1)}$$

oxidation in the troposphere by Cl contributes about 4 % of the total:

$$CH_4 + Cl \rightarrow CH_3 + HCl. \quad \text{(R2)}$$

About 8 % of methane is removed in the stratosphere by radical oxidation, such as Reactions (R2) and (R3)

$$CH_4 + O(^1D) \rightarrow CH_3 + OH. \quad \text{(R3)}$$

The rest (4 %) is removed by the soil (Kirschke et al., 2013).

Carbon and hydrogen isotopic analysis are widely used to distinguish microbial and thermal sources of atmospheric methane (e.g., Lowe et al., 1997; Ferretti et al., 2005; Tyler et al., 2007; Lassey et al., 2007). However, Reactions (R1)–(R3) produce relatively large D/H isotope effects (Saueressig et al., 1995, 1996, 2001; Crowley et al., 1999; Feilberg et al., 2005). Thus, the construction of an accurate top-down methane budget by isotopic analysis must take the isotopic signatures of both sources and sinks into account. The interpolation of methane source (and sink) fractionations represent underdetermined systems (e.g., Pohlman et al., 2009). Until recently, isotopic studies have only taken single isotopic substitutions into account. This is due to the technical challenge in measuring the low concentrations of multiply substituted, or "clumped" isotopes (e.g. $^{13}CH_3D$ which has both ^{13}C and D substitutions). Recent

ACPD
15, 27853–27875, 2015

studies (Stolper et al., 2015; Wang et al., 2015) have shown that the abundance of $^{13}CH_3D$ gives additional information about methane sources. Analysis of the clumped isotope anomaly in methane will yield unique constraints for the methane budget.

The kinetic isotope effect ${}^{j}E\alpha$ is a characteristic property of each process:

$$ {}^{j}E\alpha \equiv \frac{k({}^{i}E + OH)}{k({}^{j}E + OH)}, \quad (1) $$

where ${}^{i}E$ is the most abundant (here, the lighter) isotopologue, ${}^{j}E$ the rare (heavy) isotopologue, $k(E + OH)$ is the reaction rate coefficient for the reaction $E + OH$. As a measure of how much of an enrichment of $^{13}CH_3D$ kinetic reactions produce, the apparent clumpiness, γ is used. It is a measure of the effect of the clumped substitution on the reaction rate, as opposed to the combined effect of two single substitutions. It is defined as (Wang et al., 2015):

$$ \gamma \equiv \frac{{}^{13C,D}\alpha}{{}^{13C}\alpha \times {}^{D}\alpha} \quad (2) $$

A related measure is the $\Delta(^{13}CH_3D)$ value that quantifies the extent to which rare isotopes clump together to form a multiply substituted species, as opposed to a stochastic distribution (Ono et al., 2014):

$$ \Delta(^{13}CH_3D) \equiv \ln\left(\frac{[^{13}CH_3D][^{12}CH_4]}{[^{12}CH_3D][^{13}CH_4]}\right), \quad (3) $$

where $[^{13}CH_3D]$, $[^{12}CH_4]$, $[^{12}CH_3D]$ and $[^{13}CH_4]$ represent the concentrations of the different isotopologues.

The kinetic isotope effects for the singly substituted species CH_3D and $^{13}CH_4$ have been studied previously, both experimentally and theoretically, see Tables 1 and 2

ACPD
15, 27853–27875, 2015

respectively. The kinetic isotope effect ${}^{13C,D}\alpha$ for the reaction with OH is not described in the existing literature. The related kinetic isotope effect for the $CH_4 + Cl$ reaction was measured at room temperature with the present setup by Joelsson et al. (2014) and found to be 1.60 ± 0.04.

In the present study the kinetic isotope effects ${}^{D}\alpha$ and ${}^{13C,D}\alpha$ are determined using the relative rate method. Species concentrations in the reaction cell are determined using Fourier Transform Infrared (FTIR) spectroscopy. Further, ${}^{D}\alpha$, ${}^{13C}\alpha$, and ${}^{13C,D}\alpha$ are calculated using quantum chemistry and transition state theory.

2 Experimental procedures

2.1 Relative rate method

The experiment is carried out using the relative rate method on a semi-static gas mixture. The decaying concentrations of reactants are measured as a function of the extent of reaction. Considering two bimolecular reactions with second order rate coefficients k_A and k_B,

$$A + OH \xrightarrow{k_A} \text{Products}, \quad \text{(R4)}$$

$$B + OH \xrightarrow{k_B} \text{Products}, \quad \text{(R5)}$$

and assuming there are no other loss processes, the following relation holds:

$$\ln\left(\frac{[A]_0}{[A]_t}\right) = \frac{k_A}{k_B} \ln\left(\frac{[B]_0}{[B]_t}\right). \quad (4)$$

Here $[A]_0$, $[A]_t$, $[B]_0$ and $[B]_t$ represent the concentrations of compounds A and B at times 0 and t respectively. The slope of $\ln([A]_0/[A]_t)$ vs. $\ln([B]_0/[B]_t)$ will give the relative reaction rate coefficient. In these experiments A is ${}^{12}CH_4$ and B is ${}^{12}CH_3D$ or ${}^{13}CH_3D$.

ACPD
15, 27853–27875, 2015

2.2 Photoreactor

Experiments are carried out in the photochemical reactor at the University of Copenhagen, Department of Chemistry. The reactor has been described in detail elsewhere (Nilsson et al., 2009). It consists of a 100 L quartz cell with multi-pass optics surrounded by 16 UV-C flourescent Hg lamps in a temperature controlled housing. The cell is coupled to a Bruker IFS 66v/S FTIR spectrometer with either a mercury cadmium telluride (MCT) detector (Experiments 1–4) or an indium antimonide (InSb) (Experiments 5–16). Two thermocouple gauges are placed inside the temperature controlled housing to monitor the temperature and a pressure gauge is connected to the cell to monitor pressure inside the cell. The temperatures and the pressures are logged every 0.5 s.

The gas mix is prepared by expanding H_2O vapor (Milli-Q Ultrapure Water) into the chamber through the glass gas manifold. The two methane isotopologues CH_3D (Experiments 1–8) (purity > 98 %, Cambridge Isotope Laboratories, Inc.) or $^{13}CH_3D$ (Experiments 9–16), and CH_4 (purity > 99 %, Aldrich) and O_3 are flushed into the chamber with a N_2 buffer (purity 99.998 %, Air Liquide), all at the concentrations given in Table 3. $^{13}CH_3D$ is synthesized using the Grignard reaction, see Joelsson et al. (2014). O_3 is generated from O_2 (purity 99.97 %, Air Liquide) using an ozone generator (Model AC-20, O_3 Technology), preconcentrated before injection on silica gel cooled with ethanol and dry ice to −67 °C. The desired pressure in the cell (450 hPa) is obtained using N_2 as bathgas. The starting pressure is chosen such that the pressure is high enough for the N_2 to quench $O(^1D)$ radicals, but low enough to keep the final pressure below atmospheric pressure. The gas mixture is left to rest for up to 1.5 h while several IR spectra are recorded to ensure that no instability or dark chemistry occurs in the gas mix. The UV-C lamps are lit for up to 5 min photolysing at least 75 % of the O_3 according to:

$$O_3 + h\nu \rightarrow O(^1D) + O_2. \quad \text{(R6)}$$

ACPD
15, 27853–27875, 2015

Up to 0.2 Pa O_3 is flushed with about 20 hPa N_2 into the chamber to compensate for the loss of ozone with time, mainly due to $O(^3P) + O_3$. A pressure gradient is established and maintained throughout the filling process such that no gas leaks back from the chamber into the gasline. Spectra are recorded at each filling step. The procedure is repeated until the mix has a final pressure of 933 hPa. Two experiments are conducted at each of the temperatures 278, 288, 298, and 313 K for each of the two heavy methane istopologues. Exact temperatures are listed in Table 3. After each experiment a dilution test is performed: 133 hPa is pumped out and the chamber is refilled with 133 hPa N_2. This is repeated 5–6 times. Ideally, concentration calculations from the spectral fits (data analysis described below) of the resulting spectra should give a linear fit with the slope of 1. The slope of these dilution tests are presented in Table 3. In an extra experiment with $^{12}CH_3D$, N_2O (Air Liquide, no purity information available) is added as an $O(^1D)$ tracer. The results from this experiment are used as a spot check to validate a model that was constructed to investigate the extent of $O(^1D)$ chemistry. An example of an experiment plot can be found in Fig. S1 in the Supplement.

2.3 Data analysis

The experimental IR spectra are analyzed using the program MALT, version 5 (Griffith, 1996). The program generates a simulated spectrum from initial estimates of the absorber concentrations and instrument parameters. The residual between the experimental and simulated spectra is reduced through iteration. Simulated lineshapes are generated using HITRAN absorption parameters (version 2008) (Rothman et al., 2009) convolved with an FTIR instrument function simulating the Bruker IFS 66v/S instrument. The InSb detector covers a spectral range from 1800 to 5000 cm^{-1} and the MCT detector covers a spectral range from 400 to 5000 cm^{-1}. The concentrations of $^{12}CH_3D$ and $^{13}CH_3D$ are calculated from spectral fits in the region 2140–2302 cm^{-1}. Concentrations of $^{12}CH_4$ are calculated from spectral fits in the region 2838–2997 cm^{-1}. As there is no HITRAN data available for $^{13}CH_3D$ in

ACPD
15, 27853–27875, 2015

this region, the cross sections from 2000 to 2400 cm^{-1} for this isotopologue where estimated by shifting the spectrum of $^{12}CH_3D$, see Joelsson et al. (2014). In the region 2850–3009 cm^{-1}, temperature adjusted reference spectra of $^{13}CH_3D$ are used for the fits, together with the simulated spectra of $^{12}CH_4$ and H_2O. The spectral windows are sometimes adjusted to exclude saturated lines. Examples of spectral fits can be found in Figs. S2, S3, and S4.

After $[^xCH_3D]$ (where $x = 12$ or $x = 13$) and $[^{12}CH_4]$ are obtained from the spectral analysis, $\ln([^xCH_3D]_0/[^xCH_3D]_t)$ is plotted against $\ln([^{12}CH_4]_0/[^{12}CH_4]_t)$ as described in Sect. 2.1. A straight line is fitted to these data points using a weighted total least squares routine (York et al., 2004). The fitting procedure takes uncertainties in both dimensions into account. An example of a straight line fit can be found in Fig. S1. In the curve fitting procedure, the parameters A and B in the linearized version of the Arrhenius equation:

$$k = A \cdot \exp(B \cdot T^{-1}) \rightarrow \ln(k) = \ln(A) + B \cdot T^{-1} \quad (5)$$

is used. Also here, the method of York et al. (2004) are adjusted to match experiments. The temperature in the cell is taken as the average of the measurements from two thermocouples inside the temperature housing. These averages constitute a combined measurement series. The temperature is defined by the temporal mean of the combined temperature measurements series and the uncertainty of the temperature is the standard deviation of the combined temperature measurement series.

2.4 Kinetic model

The kinetic model, previously described and used by Nilsson et al. (2012), uses the methane reaction subset and associated (O_x and HO_x) chemistry. The Kintecus software (Ianni, 2003), simulates the photolysis of O_3 and the following oxidation chain of CH_4. A primary reason for using the model is to evaluate the influence of $O(^1D)$, Reaction (R3), which rivals Reaction (R1). To model ozone photolysis accurately, the

ACPD
15, 27853–27875, 2015

modeled O_3 is matched to the measured value, then the model is verified by comparing the decrease of CH_4 and the increase of H_2O with experiment. The model is run for each refill of O_3, the reaction rates of Reactions (R1) and (R3). The model is designed for room temperature; experiments at other temperatures are not modeled. Experiment 2 is thus modeled: 4.4 % of CH_4 is estimated to be lost to Reaction (R3). In an additional experiment N_2O was introduced in the chamber as an $O(^1D)$-tracer. Since N_2O does not react with OH and is not photolyzed at the wavelengths present (Nilsson et al., 2009), the decrease of N_2O should be only due to Reaction (R7):

$$N_2O + O(^1D) \rightarrow \text{products.} \quad \text{(R7)}$$

The amount of CH_4 lost by Reaction (R3) can therefore be approximated by:

$$1 - \frac{[CH_4]_t}{[CH_4]_0} = 1 - \exp\left(-k_{(R3)}[O(^1D)]t\right) = 1 - \frac{[N_2O]_t}{[N_2O]_0}^{(k_{(R7)}/k_{(R3)})}, \quad (6)$$

where $k_{(R7)} = 1.27 \times 10^{-10}\,\text{cm}^{-3}\,\text{s}^{-1}$ and $k_{(R3)} = 1.75 \times 10^{-10}\,\text{cm}^{-3}\,\text{s}^{-1}$ (Sander et al., 2010). This gives 2.3 % $[CH_4]$ lost by oxidation of $O(^1)$, Reaction (R3). The model estimates that 4.7 % $[CH_4]$ was lost by Reaction (R3). Both methods agree that $O(^1D)$ loss is a minor channel.

3 Theoretical procedure

Rate constants and kinetic isotope effects for $CH_4 + OH$ were calculated using a procedure similar to that employed by Joelsson et al. (2014).

3.1 Computational chemistry calculations

The geometries of reactants, products and transition states were determined using a geometry optimization procedure based on the unrestricted MP2 method (Møller and

ACPD
15, 27853–27875, 2015

Plesset, 1934) and the aug-cc-pVQZ orbital basis set (Dunning Jr., 1989; Woon and Dunning Jr., 1993). Harmonic vibrational frequencies for all relevant isotopologues of reactants, products, and transition states were obtained at the same level of theory. The calculations were carried out using the Gaussian 09 program package (Frisch et al., 2009).

The electronic energy of the optimized structures were refined using the CCSD(T) method (Watts et al., 1993; Knowles et al., 1993, 2000) with aug-cc-pVTZ, aug-cc-pVQZ, and aug-cc-pV5Z basis sets. The results from the different basis sets were used to extrapolate the electronic energy at the complete basis set limit following the approach of Halkier et al. (1998) as described by Joelsson et al. (2014). Additional information can be found in Supplement.

3.2 Rate constant calculations

The abstraction of a CH_4 hydrogen atom by OH can occur at four different sites. Depending on the methane isotopologue in question, these sites are either distinguishable or indistinguishable. Microscopic rate constants are calculated for hydrogen abstraction at each site using classical transition state theory with a tunneling correction factor,

$$k^{(i)}_{\text{mikro}} = \eta^{(i)}_{\text{tun}} \frac{k_b T}{h} \frac{Q^{(i)}_{\text{TS}}}{Q_{\text{reac}}} \exp -\Delta E^{(i)}/\text{RT} \quad (7)$$

where $\Delta E^{(i)}$ is the reaction barrier height (including the zero point vibrational energy) for the ith reaction path. $\eta^{(i)}_{\text{tun}}$ is a tunneling correction factor obtained using the Wigner tunneling correction (Wigner, 1932). $Q^{(i)}_{\text{TS}}$ and Q_{reac} are the partition functions for the transition state and reacting pair, respectively. The total rate constant is obtained by summing over the microscopic rate constants.

ACPD
15, 27853–27875, 2015

4 Results and discussion

The results of the 16 individual experiments (eight for each isotopologue) are tabulated in Table 3. The resulting $^{D}\alpha$, $^{13C}\alpha$, and $^{13C,D}\alpha$ values from the experimental and theoretical studies are tabulated in Tables 1, 2, and 4 along with previous experimental and theoretical results. The results are also shown in Figs. 1 and 2 for reactions of CH_3D and $^{13}CH_3D$ respectively.

The exponential curve fits yielded the parameters presented in Tables 1 and 4 giving $^{D}\alpha_{Arr} = 1.32 \pm 0.13$ and $^{13C,D}\alpha_{Arr} = 1.32 \pm 0.20$ at $T = 298$ K. The mean of results of room temperature experiments Experiments 1 and 2, and Experiments 9 and 10 is $^{D}\alpha_{exp} = 1.31 \pm 0.01$ and $^{13C,D}\alpha_{exp} = 1.34 \pm 0.01$ respectively. It follows that $\gamma_{exp} = 1.02 \pm 0.02$ at $T = 298$ K, using $^{13C}\alpha_{exp} = 1.0039 \pm 0.0002$ (Saueressig et al., 2001), meaning that the clumped isotope might react slower relative to what would be predicted based on the kinetic isotope effects of CH_3D and $^{13}CH_4$. However, if the Arrhenius parameters are used to calculate the kinetic isotope effects at $T = 298$ K, $\gamma_{Arr} = 1.00 \pm 0.18$ (i.e. the reaction has no clumping effect). All uncertainties are given as one standard deviation (σ). The theoretical results gives $\gamma_{theory} = 1.00$ at $T = 298$ K.

The present experimental room temperature results for $^{D}\alpha$ agree, to within the error bars, with the previous experimental studies, with the exception of DeMore (1993). DeMore (1993) used FTIR spectroscopy with a slow flow setup where the two methane isotopologues were measured seperately with a common reference compound. The low $^{D}\alpha$ value in DeMore (1993) may be explained by interference from $O(^1D)$ radicals: OH radicals were produced by photolysis of O_3 at 254 nm in the presence of H_2O, as in the present study. A relatively high rate of Reaction (R3) would reduce the final kinetic isotope effect, since the kinetic isotope effect for oxidation with $O(^1D)$ is smaller than the kinetic isotope effect for the oxidation of OH (Saueressig et al., 2001). The present experimental results of $^{D}\alpha$ are also in good agreement with Masgrau et al. (2001) and Sellevåg et al. (2006). The theoretical calculations of $^{D}\alpha$ give a slightly

ACPD
15, 27853–27875, 2015

higher value than the experimental results, although they are in good agreement with the best Arrhenius curve fit at $T = 298\,K$.

The experimental room temperature result for $^{13C,D}\alpha$ agrees to within the error bar with both the theoretical value and the best estimate of the Arrhenius curve fit at $T = 298\,K$.

The theoretical calculations show a very small temperature dependence; the variability in the experimental data is large compared to the value of the slope, making a quantification of the temperature dependence uncertain. The $^{D}\alpha$ value of Gordon and Mulac (1975) seems to deviate substantially from an extrapolation of the current Arrhenius expression; it has previously been pointed out that this value includes some inconsistencies (DeMore, 1993).

At steady state, assuming no clumping in emissions, $\Delta(^{13}CH_3D) = \ln(\gamma)$. It follows that $\Delta(^{13}CH_3D) = 0.02 \pm 0.02$ implying that the clumped isotope effect of the OH reaction is very small.

Furthermore, the theoretical analysis revealed that the primary cause for the kinetic isotope effect is the substantially reduced reactivity of the D atom, which, in turn, can be explained by a significant increase in reaction barrier due to changes in vibrational zero point energy and to a lesser extent tunneling.

5 Conclusions

We present experimentally derived $CH_4 + OH$ kinetic isotope effects and their temperature dependence for CH_3D and $^{13}CH_3D$; the latter is reported for the first time. We find $^{D}\alpha = 1.31 \pm 0.01$ and $^{13C,D}\alpha = 1.34 \pm 0.03$ at room temperature, implying that the kinetic isotope effect is multiplicative such that $\gamma = 1$ to within the experimental uncertainty. We compare our experimental results to theoretical estimates derived using transition state theory with tunneling correction and kinetic isotope effects reported in the literature. We find good agreement with theory and literature values.

ACPD
15, 27853–27875, 2015

Based on these experiments we find that the OH reaction (the main sink of methane) at steady-state has a $\Delta(^{13}CH_3D) = 0.02 \pm 0.02$.

The Supplement related to this article is available online at doi:10.5194/acpd-15-27853-2015-supplement.

Acknowledgements. This research has recieved funding from the European Community's Seventh Framework Programme (FP7/2007-2013) under grant agrement No. 237890, the Carlsberg foundation, and the Danish Counsil for Independent Research.

References

Cantrell, C., Shetter, R., Mcdaniel, A., Calvert, J., Davidson, J., Lowe, D., Tyler, S., Cicerone, R., and Greenberg, J.: Carbon kinetic isotope effect in the oxidation of methane by the hydroxyl radical, J. Geophys. Res., 95, 22455–22462, 1990. 27871

Ciais, P., Sabine, C., Bala, G., Bopp, L., Brovkin, V., Canadell, J., Chhabra, A., DeFries, R., Galloway, J., Heimann, M., Jones, C., Le Quéré, C., Myneni, R., Piao, S., and Thornton, P.: Carbon and other biogeochemical cycles, in: Climate Change 2013: The Physical Science Basis. Contribution of Working Group I to the Fifth Assessment Report of the Intergovernmental Panel on Climate Change, Cambridge, United Kingdom and New York, NY, USA, 2013. 27855

Crowley, J. N., Saueressig, G., Bergamaschi, P., Fischer, H., and Harris, G. W.: Carbon kinetic isotope effect in the reaction $CH_4 + Cl$: a relative rate study using FTIR spectroscopy, Chem. Phys. Lett., 303, 268–274, 1999. 27855

DeMore, W.: Rate constant ratio for the reactions of OH with CH_3D and CH_4, J. Phys. Chem.-US, 97, 8564–8566, 1993. 27863, 27864, 27870

Dunning Jr., T. H.: Gaussian basis sets for use in correlated molecular calculations. I. The atoms boron through neon and hydrogen, J. Chem. Phys., 90, 1007–1023, 1989. 27862

Feilberg, K. L., Griffith, D. W. T., Johnson, M. S., and Nielsen, C. J.: The ^{13}C and D kinetic isotope effects in the reaction of CH_4 with Cl, Int. J. Chem. Kinet., 37, 110–118, 2005. 27855

ACPD
15, 27853–27875, 2015

Ferretti, D. F., Miller, J. B., White, J. W. C., Etheridge, D. M., Lassey, K. R., Lowe, D. C., Meure, C. M. M., Dreier, M. F., Trudinger, C. M., van Ommen, T. D., and Langenfelds, R. L.: Unexpected changes to the global methane budget over the past 2000 years, Science, 309, 1714–1717, 2005. 27855

Frisch, M. J., Trucks, G. W., Schlegel, H. B., Scuseria, G. E., Robb, M. A., Cheeseman, J. R., Scalmani, G., Barone, V., Mennucci, B., Petersson, G. A., Nakatsuji, H., Caricato, M., Li, X., Hratchian, H. P., Izmaylov, A. F., Bloino, J., Zheng, G., Sonnenberg, J. L., Hada, M., Ehara, M., Toyota, K., Fukuda, R., Hasegawa, J., Ishida, M., Nakajima, T., Honda, Y., Kitao, O., Nakai, H., Vreven, T., Montgomery Jr., J. A., Peralta, J. E., Ogliaro, F., Bearpark, M., Heyd, J. J., Brothers, E., Kudin, K. N., Staroverov, V. N., Kobayashi, R., Normand, J., Raghavachari, K., Rendell, A., Burant, J. C., Iyengar, S. S., Tomasi, J., Cossi, M., Rega, N., Millam, J. M., Klene, M., Knox, J. E., Cross, J. B., Bakken, V., Adamo, C., Jaramillo, J., Gomperts, R., Stratmann, R. E., Yazyev, O., Austin, A. J., Cammi, R., Pomelli, C., Ochterski, J. W., Martin, R. L., Morokuma, K., Zakrzewski, V. G., Voth, G. A., Salvador, P., Dannenberg, J. J., Dapprich, S., Daniels, A. D., Farkas, O., Foresman, J. B., Ortiz, J. V., Cioslowski, J., and Fox, D. J.: Gaussian 09 Revision A.1, Gaussian, Inc., Wallingford CT, 2009. 27862

Gierczak, T., Talukdar, R. K., Herndon, S. C., Vaghjiani, G. L., and Ravishankara, A. R.: Rate coefficients for the reactions of hydroxyl radicals with methane and deuterated methanes, J. Phys. Chem. A, 101, 3125–3134, 1997. 27870, 27874

Gordon, S. and Mulac, W. A.: Reaction of OH(X2-PI) radical produced by pulse-radiolysis of water-vapor, Int. J. Chem. Kinet., 1, 289–299, 1975. 27864, 27870

Griffith, D. W. T.: Synthetic calibration and quantitative analysis of gas-phase FT-IR spectra, Appl. Spectrosc., 50, 59–70, 1996. 27859

Gupta, M. L., McGrath, M. P., Cicerone, R. J., Rowland, F. S., and Wolfsberg, M.: C-12/C-13 kinetic isotope effects in the reactions of CH_4 with OH and Cl, Geophys. Res. Lett., 24, 2761–2764, 1997. 27871

Halkier, A., Helgaker, T., Jørgensen, P., Klopper, W., Koch, H., Olsen, J., and Wilson, A. K.: Basis-set convergence in correlated calculations on Ne, N_2, and H_2O, Chem. Phys. Lett., 286, 243–252, 1998. 27862

Ianni, J.: A Comparison of the Bader–Deuflhard and the Cash–Karp Runge–Kutta Integrators for the GRI-MECH 3.0 Model Base on the Chemical Kinetics Code Kintecus, Elsevier Science Ltd., Oxford, UK, 2003. 27860

ACPD
15, 27853–27875, 2015

IPCC: Climate Change 2013: The Physical Science Basis. Contribution of Working Group I to the Fifth Assessment Report of the Intergovernmental Panel on Climate Change, Cambridge University Press, Cambridge, United Kingdom and New York, NY, USA, 2013. 27854, 27855

Joelsson, L. M. T., Forecast, R., Schmidt, J. A., Meusinger, C., Nilsson, E. J. K., Ono, S., and Johnson, M. S.: Relative rate study of the kinetic isotope effect in the (CH_3D)-C-13 + Cl reaction, Chem. Phys. Lett., 605, 152–157, 2014. 27857, 27858, 27860, 27861, 27862

Kirschke, S., Bousquet, P., Ciais, P., et al.: Three decades of global methane sources and sinks, Nat. Geosci., 6, 813–823, 2013. 27855

Knowles, P. J., Hampel, C., and Werner, H.-J.: Coupled cluster theory for high spin, open shell reference wave functions, J. Chem. Phys., 99, 5219–5227, 1993. 27862

Knowles, P. J., Hampel, C., and Werner, H.-J.: Erratum: "Coupled cluster theory for high spin, open shell reference wave functions" [J. Chem. Phys. 99, 5219 (1993)], J. Chem. Phys., 112, 3106–3107, 2000. 27862

Lasaga, A. C. and Gibbs, G.: Ab initio studies of the kinetic isotope effect of the $CH_4 + OH$· atmospheric reaction, Geophys. Res. Lett., 18, 1217–1220, 1991. 27871

Lassey, K. R., Etheridge, D. M., Lowe, D. C., Smith, A. M., and Ferretti, D. F.: Centennial evolution of the atmospheric methane budget: what do the carbon isotopes tell us?, Atmos. Chem. Phys., 7, 2119–2139, doi:10.5194/acp-7-2119-2007, 2007. 27855

Lowe, D. C., Manning, M. R., Brailsford, G. W., and Bromley, A. M.: The 1991–1992 atmospheric methane anomaly: Southern Hemisphere C-13 decrease and growth rate fluctuations, Geophys. Res. Lett., 24, 857–860, 1997. 27855

Masgrau, L., Gonzalez-Lafont, A., and Lluch, J. M.: The reactions $CH_nD_{4-n}+OH \rightarrow P$ and $CH_4 + OD \rightarrow CH_3 + HOD$ as a test of current direct dynamics multicoefficient methods to determine variational transition state rate constants. II, J. Chem. Phys., 115, 4515–4526, 2001. 27863, 27870

Melissas, V. S. and Truhlar, D. G.: Deuterium and C-13 kinetic isotope effects for the reaction of OH with CH_4, J. Chem. Phys., 99, 3542–3552, 1993. 27871

Møller, C. and Plesset, M. S.: Note on an approximation treatment for many-electron systems, Phys. Rev., 46, 618–622, 1934. 27861

Nilsson, E. J. K., Eskebjerg, C., and Johnson, M. S.: A photochemical reactor for studies of atmospheric chemistry, Atmos. Environ., 43, 3029–3033, 2009. 27858, 27861

ACPD
15, 27853–27875, 2015

Nilsson, E. J. K., Andersen, V. F., Nielsen, O. J., and Johnson, M. S.: Rate coefficients for the chemical reactions of CH_2F_2, $CHClF_2$, CH_2FCF_3 and CH_3CCl_3 with $O(^1D)$ at 298 K, Chem. Phys. Lett., 554, 27–32, 2012. 27860

NIST: National Institute of Standards and Technology Chemical Kinetics Database, available at: http://kinetics.nist.gov, last access: 2 October 2015, 2015. 27870

Ono, S., Wang, D. T., Gruen, D. S., Sherwood Lollar, B., Zahniser, M. S., McManus, B. J., and Nelson, D. D.: Measurement of a doubly substituted methane isotopologue, $^{13}CH_3D$, by tunable infrared laser direct absorption spectroscopy, Anal. Chem., 86, 6487–6494, 2014. 27856

Pohlman, J., Kaneko, M., Heuer, V., Coffin, R., and Whiticar, M.: Methane sources and production in the northern Cascadia margin gas hydrate system, Earth Planet. Sc. Lett., 287, 504–512, 2009. 27855

Rothman, L. S., Gordon, I. E., Barbe, A., Benner, Bernath, P. F., Birk, M., Boudon, V., Brown, L. R., Campargue, A., and Champion, J. P.: The HITRAN 2008 molecular spectroscopic database, J. Quant. Spectrosc. Ra., 110, 533–572, 2009. 27859

Rust, F. and Stevens, C.: Carbon kinetic isotope effect in the oxidation of methane by hydroxyl, Int. J. Chem. Kinet., 12, 371–377, 1980. 27871

Sander, S. P., Friedl, R., Barker, J., et al.: Chemical kinetics and photochemical data for use in atmospheric studies: evaluation number 17, National Aeronautics and Space Administration, Jet Propulsion Laboratory, California Institute of Technology Pasadena, CA, 2010. 27861

Saueressig, G., Bergamaschi, P., Crowley, J. N., Fischer, H., and Harris, G. W.: Carbon kinetic isotope effect in the reaction of CH_4 with Cl atoms, Geophys. Res. Lett., 22, 1225–1228, 1995. 27855

Saueressig, G., Bergamaschi, P., Crowley, J. N., Fischer, H., and Harris, G. W.: D/H kinetic isotope effect in the reaction $CH_4 + Cl$, Geophys. Res. Lett., 23, 3619–3622, 1996. 27855

Saueressig, G., Crowley, J. N., Bergamaschi, P., Bruhl, C., Brenninkmeijer, C. A. M., and Fischer, H.: Carbon 13 and D kinetic isotope effects in the reactions of CH_4 with O(D-1) and OH: New laboratory measurements and their implications for the isotopic composition of stratospheric methane, J. Geophys. Res.-Atmos., 106, 23127–23138, 2001. 27855, 27863, 27870, 27871

Sellevåg, S. R., Nyman, G., and Nielsen, C. J.: Study of the carbon-13 and deuterium kinetic isotope effects in the Cl and OH reactions of CH_4 and CH_3Cl, J. Phys. Chem. A, 110, 141–152, 2006. 27863, 27870, 27871

ACPD
15, 27853–27875, 2015

Stolper, D., Martini, A., Clog, M., Douglas, P., Shusta, S., Valentine, D., Sessions, A., and Eiler, J.: Distinguishing and understanding thermogenic and biogenic sources of methane using multiply substituted isotopologues, Geochim. Cosmochim. Ac., 161, 219–247, 2015. 27856

Tyler, S. C., Rice, A. L., and Ajie, H. O.: Stable isotope ratios in atmospheric CH_4: Implications for seasonal sources and sinks, J. Geophys. Res., 112, D03303, doi:10.1029/2006JD007231, 2007. 27855

Wang, D. T., Gruen, D. S., Lollar, B. S., Hinrichs, K.-U., Stewart, L. C., Holden, J. F., Hristov, A. N., Pohlman, J. W., Morrill, P. L., Koenneke, M., Delwiche, K. B., Reeves, E. P., Sutcliffe, C. N., Ritter, D. J., Seewald, J. S., McIntosh, J. C., Hemond, H. F., Kubo, M. D., Cardace, D., Hoehler, T. M., and Ono, S.: Nonequilibrium clumped isotope signals in microbial methane, Science, 348, 428–431, 2015. 27856

Watts, J. D., Gauss, J., and Bartlett, R. J.: Coupled-cluster methods with noniterative triple excitations for restricted open-shell Hartree–Fock and other general single determinant reference functions. Energies and analytical gradients, J. Chem. Phys., 98, 8718–8733, 1993. 27862

Wigner, E.: On the quantum correction for thermodynamic equilibrium, Phys. Rev., 40, 749, doi:10.1103/PhysRev.40.749, 1932. 27862

Woon, D. E. and Dunning Jr., T. H.: Gaussian basis sets for use in correlated molecular calculations. III. The atoms aluminum through argon, J. Chem. Phys., 98, 1358–1371, 1993. 27862

York, D., Evensen, N. M., Martínez, M. L., and De Basable Delgado, J.: Unified equations for the slope, intercept, and standard errors of best straight line, Am. J. Phys., 72, 367–375, 2004. 27860

ACPD
15, 27853–27875, 2015

Table 1. Experimental and theoretical studies of ${}^{D}\alpha$. The temperature dependence studies are presented in the Arrhenius form ${}^{D}\alpha(T) = A(T/298\,\mathrm{K})^{n}\exp(BT^{-1})$, where A, n, and B are tabulated, T is the given temperature range, and ${}^{D}\alpha(T = 298\,\mathrm{K})$ is the resulting kinetic isotope effect at $T = 298\,\mathrm{K}$. Where no B coefficient is presented A can be taken as ${}^{D}\alpha(T)$ for the given temperature range. All uncertainties are given as one standard deviation (σ).

Study	A	n	B (K)	T (K)	${}^{D}\alpha(T = 298\,\mathrm{K})$
Experimental studies					
Present study[a]	1.23 ± 0.08	0	21 ± 21	[278, 313]	1.31 ± 0.01[h]
Saueressig et al. (2001) [b]	1.294 ± 0.009	–	–	296	–
Gierczak et al. (1997) [c]	1.09 ± 0.05	0	49 ± 11	[220, 415]	1.25 ± 0.07
DeMore (1993) [a]	0.91	0	75	[298, 360]	1.17
Gordon and Mulac (1975) [d]	1.50	–	–	416	–
Gordon and Mulac (1975) [d, i]	1.06	–	–	416	–
Theoretical studies					
Present study[e]	1.314	0	6.354	[200, 300]	1.339
Sellevåg et al. (2006) [f]	[1.30, 1.00]	–	–	[200, 1500]	1.27
Masgrau et al. (2001) [g, j]	1.00	−0.02	50.5	[200, 1500]	1.25

[a] Fourier transform infrared spectroscopy – relative rate.
[b] Tunable Diode Laser Absorption Spectroscopy – isotope ratio mass spectrometry.
[c] Pulsed photolysis – pulsed laser-induced flourescence.
[d] Pulse radiolysis.
[e] Transition state theory with Wigner tunneling correction.
[f] Canonical unified statistical theory.
[g] Multicoefficient correlation method.
[h] Average room temperature value, not obatined from curve fit.
[i] Re-evaluated by DeMore (1993).
[j] Arrhenius parameters available at NIST (2015).

ACPD
15, 27853–27875, 2015

Table 2. Experimental and theoretical studies of $^{13}C\alpha$. The temperature dependence studies are presented in the Arrhenius form $^{13}C\alpha(T) = A\exp(BT^{-1})$, where A and B are tabulated, T is the given temperature range, and $^{13}C\alpha(T = 298\,K)$ is the resulting kinetic isotope effect at $T = 298\,K$. Where no B coefficient is presented A can be taken as $^{13}C\alpha(T)$ for the given temperature range. All uncertainties are given as one standard deviation (σ).

Study	A	B (K)	T (K)	$^{D}\alpha(T = 298\,K)$
Experimental studies				
Saueressig et al. (2001) [a]	1.0039 ± 0.0002	–	296	–
Cantrell et al. (1990) [c]	1.0054 ± 0.0005	–	[273, 353]	1.0054 ± 0.0005
Rust and Stevens (1980) [d,i]	1.003	–	–	–
Theoretical studies				
Present study[b]	1.0137	−1.219	[200, 300]	1.0094
Sellevåg et al. (2006) [e]	[1.014, 1.00]	–	[200, 1500]	1.003
Gupta et al. (1997) [f]	1.010	–	300	–
Melissas and Truhlar (1993) [g]	[1.005, 1.001]	–	[223, 416]	1.005
Lasaga and Gibbs (1991) [h]	[1.0036, 1.0076]	–	[150, 350]	–

[a] Tunable Diode Laser Absorption Spectroscopy – isotope ratio mass spectrometry
[b] Transition state theory with Wigner tunneling correction.
[c] Gas chromatography – mass spectrometry.
[d] Isotope ratio mass spectrometry.
[e] Canonical variational transition state theory.
[f] Conventional transition state theory.
[g] Interpolated variational transition state theory with centrifugal-dominant, small-curvature tunneling coefficients.
[h] Ab initio calculations.
[i] No temperature information available.

ACPD
15, 27853–27875, 2015

Table 3. List of experiments. The experiment numbers are listed in column Exp., the detector in the column Detector, the heavy CH_4 isotopologue included in the experiments are listed in column Isotop., the mean measured temperatures in the photoreactor are listed in column T, the H_2O-vapour concentrations at the start of the experiments ($t = 0$) as obtain from spectral fitting are listed in column $[H_2O]_{t=0}$, the mean O_3 concentration after refill (i.e. the "top"-values) as obtain from spectral fitting are listed in column $[O_3]_{top}$, the kinetic isotope effect corresponding to the isotopologue are listed in column α, and the result of the dilution experiments are listed in column k_{dil}.

Exp.	Detector	Isotop.	T (K)	$[H_2O]_{t=0}$ (hPa)	$[O_3]_{top}$ (hPa)	α	k_{dil}
1	MCT	CH_3D	298.2 ± 1.2	7.1	–[a]	1.302 ± 0.038	1.011 ± 0.048
2	MCT	CH_3D	297.6 ± 0.8	5.6	0.19	1.314 ± 0.020	–[b]
3	MCT	CH_3D	277.2 ± 0.2	5.2	0.29	1.294 ± 0.017	0.962 ± 0.037
4	MCT	CH_3D	277.0 ± 0.2	5.1	0.16	1.335 ± 0.017	–[b]
5	InSb	CH_3D	284.5 ± 0.1	7.2	0.26	1.334 ± 0.012	0.999 ± 0.009
6	InSb	CH_3D	291.1 ± 0.2	7.4	–[a]	1.323 ± 0.010	0.998 ± 0.010
7	InSb	CH_3D	313.5 ± 1.3	7.1	0.17	1.301 ± 0.007	1.006 ± 0.031
8	InSb	CH_3D	312.4 ± 0.9	4.3	–[a]	1.338 ± 0.010	–[b]
9	InSb	$^{13}CH_3D$	298.5 ± 0.1	5.1	–[a]	1.359 ± 0.022	1.000 ± 0.029
10	InSb	$^{13}CH_3D$	297.6 ± 0.6	6.4	0.13	1.314 ± 0.007	0.990 ± 0.064
11	InSb	$^{13}CH_3D$	276.8 ± 0.8	5.4	–[a]	1.357 ± 0.046	1.016 ± 0.031
12	InSb	$^{13}CH_3D$	277.2 ± 1.3	5.1	–[a]	1.344 ± 0.013	1.008 ± 0.030
13	InSb	$^{13}CH_3D$	287.4 ± 1.2	5.4	–[a]	1.346 ± 0.025	1.009 ± 0.022
14	InSb	$^{13}CH_3D$	287.4 ± 0.4	4.5	–[a]	1.342 ± 0.015	1.011 ± 0.019
15	InSb	$^{13}CH_3D$	314.4 ± 1.0	5.2	0.26	1.316 ± 0.016	1.003 ± 0.038
16	InSb	$^{13}CH_3D$	313.8 ± 0.8	8.3	0.17	1.331 ± 0.033	1.001 ± 0.034

[a] Spectra recorded during or after photolysis, $[O_3]_{top}$ not available.

[b] No dilution test performed.

ACPD
15, 27853–27875, 2015

Table 4. Experimental and theoretical studies of $^{13C,D}\alpha$. The temperature dependencies are presented in the Arrhenius form $^{13C,D}\alpha(T) = A\exp(BT^{-1})$, where A and B are tabulated, T is the given temperature range, and $^{13C,D}\alpha(T = 298\,\mathrm{K})$ is the resulting kinetic isotope effect at $T = 298\,\mathrm{K}$. All uncertainties are given as one standard deviation (σ).

Study	A	B (K)	T (K)	$^{D}\alpha(T = 298\,\mathrm{K})$
Experimental study[a]	1.18 ± 0.10	38 ± 26	[278, 313]	1.34 ± 0.03[c]
Theoretical study[b]	1.328	5.301	[200, 300]	1.349

[a] Fourier transform infrared spectroscopy – relative rate.
[b] Transition state theory with Wigner tunneling correction.
[c] Average room temperature value, not obatined from curve fit.

ACPD
15, 27853–27875, 2015

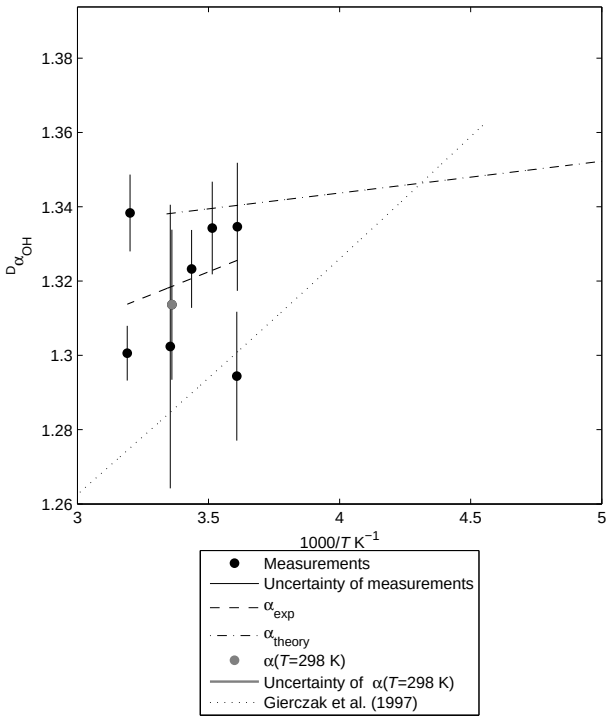

Figure 1. The individual measurements of $^{D}\alpha$, are represented by points; the accompaning individual error bars are represented by thin black solid lines; the experimental Arrhenius curve fit is represented by a dashed line; the theoretical Arrhenius curve fit is represented by a dashed-dotted line; the mean of the room temperature measurements are represented by a gray solid circle; the uncertainty of the room temperature measurements are represented by a thick gray solid line; the result from Gierczak et al. (1997) (which is included for comparison) are represented by a dotted line. All uncertainties are given as one standard deviation (σ).

ACPD
15, 27853–27875, 2015

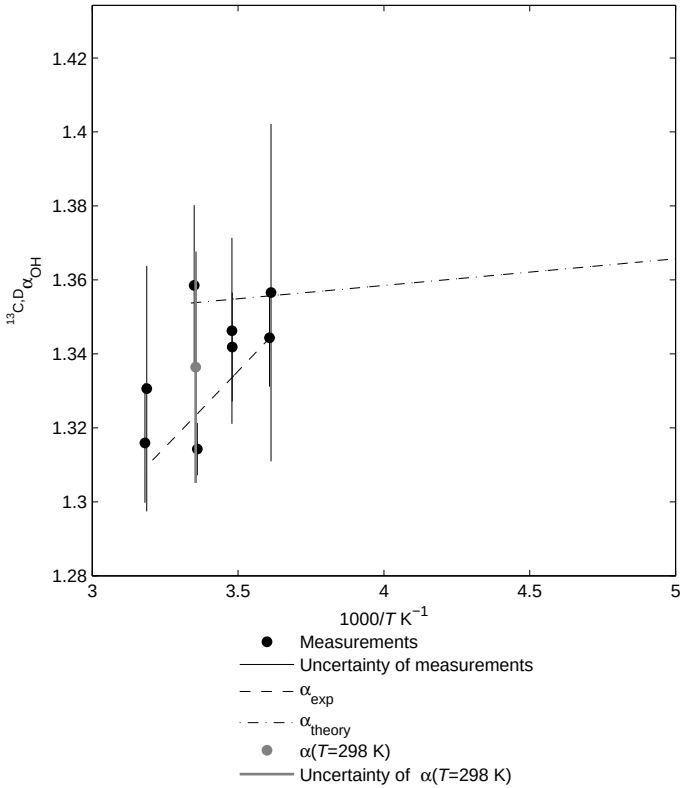

Figure 2. The individual measurements of $^{13C,D}\alpha$, are represented by points; the accompaning individual error bars are represented by thin black solid lines; the experimental Arrhenius curve fit is represented by a dashed line; the theoretical Arrhenius curve fit is represented by a dashed-dotted line; the mean of the room temperature measurements are represented by a gray solid circle; the uncertainty of the room temperature measurements are represented by a thick gray solid line. All uncertainties are given as one standard deviation (σ).

ACPD
15, 27853–27875, 2015